Journal of Power Sources 195 (2010) 5246–5251

Contents lists available at ScienceDirect

Journal of Power Sources

journal homepage: www.elsevier.com/locate/jpowsour

Performance of carbon nanofiber supported Pd–Ni catalysts for electro-oxidation of ethanol in alkaline medium

T. Maiyalagan, Keith Scott*

School of Chemical Engineering & Advanced Materials, University of Newcastle upon Tyne, Newcastle upon Tyne NE1 7RU, United Kingdom

ARTICLE INFO

Article history:
Received 5 August 2009
Received in revised form 18 January 2010
Accepted 6 March 2010
Available online 15 March 2010

Keywords:
Ethanol electro-oxidation
Pd–Ni
Nanostructured materials
Electro-catalyst
Fuel cell

ABSTRACT

Carbon nanofibers (CNF) supported Pd–Ni nanoparticles have been prepared by chemical reduction with $NaBH_4$ as a reducing agent. The Pd–Ni/CNF catalysts were characterized by X-ray diffraction (XRD), scanning electron microscopy (SEM), transmission electron microscopy (TEM) and electrochemical voltammetry analysis. TEM showed that the Pd–Ni particles were quite uniformly distributed on the surface of the carbon nanofiber with an average particle size of 4.0 nm. The electro-catalytic activity of the Pd–Ni/CNF for oxidation of ethanol was examined by cyclic voltammetry (CV). The onset potential was 200 mV lower and the peak current density four times higher for ethanol oxidation for Pd–Ni/CNF compared to that for Pd/C. The effect of an increase in temperature from 20 to 60 °C had a great effect on increasing the ethanol oxidation activity.

1. Introduction

Recently there has been increased interest in the development of direct ethanol fuel cells (DEFC). Ethanol is an interesting alternative renewable fuel which has an energy density of 8030 W h kg^{-1}; greater than that of methanol (6100 W h kg^{-1}), if complete oxidation to CO_2 is attained [1]. However, in acidic environments the complete oxidation of ethanol is difficult to achieve and attention has been directed to higher pH. The catalysts for ethanol oxidation can be more active in alkaline medium compared to acid medium [2–5]. Ethanol electro-oxidation by Pt [6–8] in alkaline solution has been reported. However, the high cost and limited supply of Pt constitute a major limitation to development of DEFC. In order to reduce the cost of catalysts, Pt-free materials such as Pd have been recently studied [9,10]. Data show that Pd is a good electro-catalyst for ethanol oxidation in alkaline media [11].

A great deal of interest has recently been focused on materials cheaper than platinum and the use of non-noble transition metals in alkaline media; in particular the performance of alloys of palladium with non-noble metals for electro-oxidation of ethanol [12]. Ethanol electro-oxidation by Ni [13] and Cu–Ni [14] in alkaline solution has been reported. Ni hollow spheres are promising electro-catalysts for alcohol oxidation in alkaline media [15]. In alkaline solutions nickel can be easily converted to $Ni(OH)_2$ and the Ni^{2+}/Ni^{3+} redox centers show high catalytic activity towards the oxidation of some small organic compounds.

In addition to development of efficient electro-catalysts for ethanol oxidation research has considered the role and use of alternative catalysts supports. Graphite nanofiber (GNF) [16], carbon nanotubes (CNT) [17–20], carbon nanohorns [21] and carbon nanocoils [22] provide alternate candidates of carbon support for fuel cell applications. Due to the high electric conductivity and structural properties, carbon nanofibers have been considered as promising catalyst support materials in fuel cell electrodes [23,24].

In this work, synthesis of Pd–Ni/CNF based catalysts are explored for possible use in DEFC in view of the good electro-catalytic activity of Pd and the ability of Ni to adsorb OH^- ions in the form of $Ni(OH)_2$ [25]. The presence of Ni species is expected to assist in the electro-oxidation of poisonous reaction intermediates adsorbed on the active Pd sites. Additionally, the use of Ni enables a reduction in catalyst cost [34].

2. Experimental

2.1. Materials

All the chemicals used were analytical grade. Vapor-grown carbon nanofibers were purchased from Pyrograf Products Inc. (OH, USA. Products PR24-LHT). Extensive characterization of representative commercially available Pyrograf carbon nanofiber has been reported [26,27]. Palladium chloride and nickel chloride hydrate were procured from Sigma–Aldrich and used as received. Ethanol and KOH were obtained from Fischer chemicals. 20%Pd/C carbon

* Corresponding author. Tel.: +44 191 2225207; fax: +44 191 2225292.
E-mail addresses: maiyalagan@gmail.com (T. Maiyalagan), K.Scott@ncl.ac.uk (K. Scott).

0378-7753/$ – see front matter © 2010 Elsevier B.V. All rights reserved.
doi:10.1016/j.jpowsour.2010.03.022

black was purchased from (E-TEK, USA); Nafion 5 wt.% solution was obtained from Sigma–Aldrich and was used as received.

2.2. Preparation of 20% Pd–Ni (3:1)/CNF catalyst

The as-received CNF was treated with aqueous solution of HNO_3 under magnetic stirring for 24 h [28]. The oxidized fibers were then repeatedly washed with distilled water to remove residual acid and evaporated to dryness.

The required amount of $PdCl_2$ and $NiCl_2{\cdot}6H_2O$, were added to 10 ml of water and 60 mg functionalized CNF were mixed by magnetic stirring for 3 h to achieve 20% Pd loading. Excess, dilute $NaBH_4$ solution was added to the solution to reduce the Pd and Ni species to form electro-catalyst. After that electro-catalyst was repeatedly washed with distilled water to remove residual salts, centrifuged and dried at 70 °C. The catalyst obtained is the Pd–Ni/CNF catalyst with 20 wt.% Pd and the atomic ratio of Pd:Ni = 3:1.

2.3. Catalyst characterization

Scanning electron microscopy (SEM) and energy dispersive X-ray (EDX) measurements were carried out using a JEOL JSM-5300LV scanning electron microscope with a ROUTEC UHV Dewar Detector at an acceleration voltage of 25 kV. Powder X-ray diffraction was recorded on a PAN analytical X'Pert Pro MPD diffractometer using CuK_α radiation. For transmission electron microscopic studies, catalysts dispersed in ethanol were placed on the copper grid and the images were obtained using Phillips CM100 transmission electron microscope, operating at an accelerating voltage of 100 keV.

2.4. Electrochemical measurements

Glassy carbon (GC) (BAS) electrode (0.07 cm^2) was polished to a mirror finish with 0.05 μm alumina suspensions before each experiment and served as substrate for the working electrode. The working electrodes were fabricated by coating catalyst ink onto a glassy carbon electrode. The catalysts ink was prepared by dispersing 35 mg of the catalyst in 0.8 cm^3 of deionized water, and 0.2 cm^3 of 5 wt.% Nafion solution and ultrasonicated for 20 min. Nafion was used simply as a binder. A known amount of suspension was added to the glassy carbon (GC) electrode and slowly dried in air. The loading of the noble metal catalyst was 0.3 mg cm^{-2}. A solution of 1.0 mol dm^{-3} (M) ethanol in 1 M KOH was used to study ethanol oxidation activity.

Electrochemical measurements were collected using a computer controlled Gill AC potentiostat (ACM Instruments Ltd., Cumbria, UK). All experiments were carried out in a three-electrode glass cell, incorporating the glassy carbon working electrode, a mercury–mercury oxide reference electrode and a platinum mesh (25 mm × 25 mm) counter electrode. All the electrochemical experiments were carried out at room temperature in 1 M KOH electrolyte. The electrolyte solution was purged with high purity nitrogen for 30 min prior to a series of voltammetric experiments. The catalytic performance was observed in 1 mol dm^{-3} KOH solution, 1 M ethanol at pH 14. Current densities were calculated based

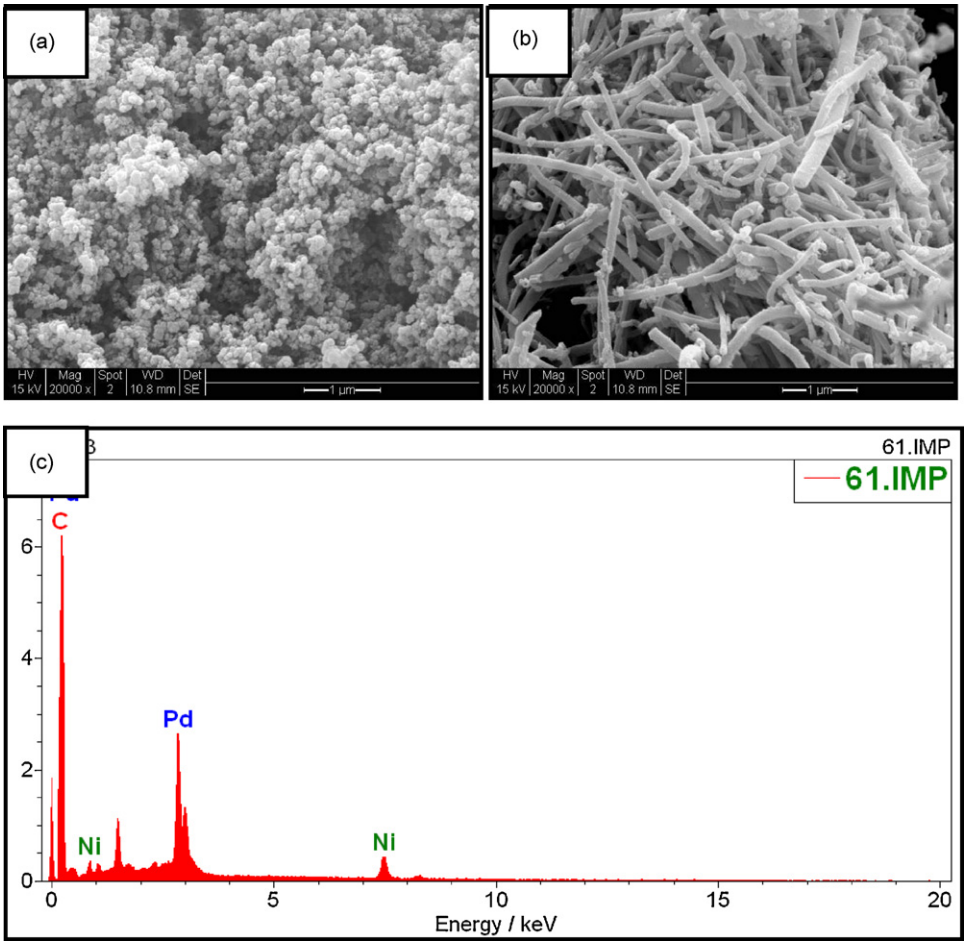

Fig. 1. SEM images of (a) Pd/C, (b) Pd–Ni/CNF and (c) EDX spectra of Pd–Ni/CNF catalysts.

on the geometric area of the electrode. Triply distilled water was used throughout for the preparation of solutions.

3. Results and discussion

The micrograph of the Pd/C and Pd–Ni/CNF electrodes have been investigated by SEM (Fig. 1) and the EDX spectrum for Pd–Ni/CNF is presented in Fig. 1c respectively. The agglomerated globular morphology of Pd/C resulted in rough surface with larger particles. The surface morphology of Pd–Ni/CNF catalysts was found to be uniform and tubular walls are sufficiently decorated with nanoparticles. EDX analysis confirmed the presence of Pd and Ni in the Pd–Ni/CNF catalyst. According to the EDX measurements (Fig. 1c), Pd–Ni/CNF catalyst prepared in this work contained 20.1 wt.% of Pd with a Pd/Ni atomic ratio of 3:1.0–1.1, which agrees well with the stoichiometric ratio of 3:1 used in the starting mixture.

Fig. 2 shows the XRD profiles of the Pd/C (curve a) and Pd–Ni/CNFs (curve b) catalysts. XRD patterns reveal the bulk structure of the catalyst and its support. It can be seen that the first peak located at a 2θ value of about 26° is referred to carbon (0 0 2). The other four peaks are characteristic of face centered cubic (fcc) crystalline Pd (JCPDS, Card No. 05-0681), corresponding to the planes (1 1 1), (2 0 0), (2 2 0) and (3 1 1) at 2θ values of about, 47°, 68° and 82°. The nickel particles are air-sensitive, both in the stable suspension and in the solid state. The presence of the oxide phase NiO (reflections (2 0 0) and (2 2 0)) can be observed on the electron diffraction pattern [29]. The average particle sizes of the catalyst were calculated from Pd (2 2 0) peak by the Scherrer formula [30]:

$$d\,(\text{Å}) = \frac{k\lambda}{\beta \cos\theta}$$

where k is a coefficient (0.9), λ the wavelength of X-ray used (1.54056 Å), β the full-width half maximum and θ is the angle at position of peak maximum.

The mean particle size obtained from the XRD patterns were 2.9 nm for Pd/C and 2.5 nm for Pd–Ni/CNF. Typical TEM images of the Pd/C and Pd–Ni/CNF catalysts (Fig. 3) show an average particle size of 4.8 and 4.0 nm for Pd/C and Pd–Ni/CNF respectively. Thus, the values of the mean particle size obtained from XRD are slightly lower than that obtained from TEM analysis. Although some agglomeration of Pd nanoparticles occurred on the Vulcan support, it can be seen from the TEM image that Pd particles dispersion was

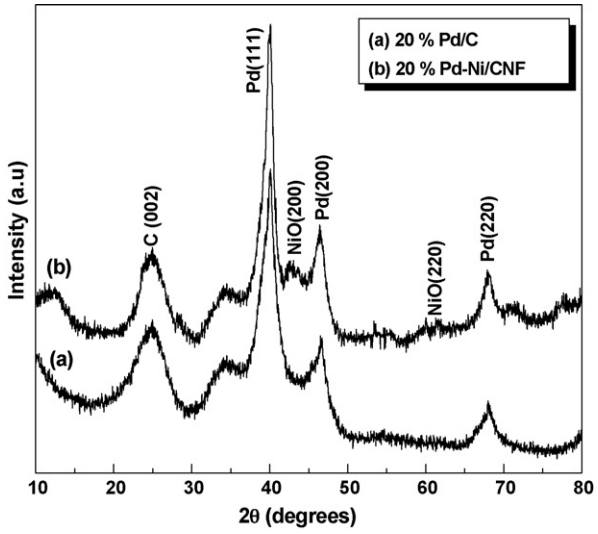

Fig. 2. XRD patterns of (a) Pd/C and (b) Pd–Ni/CNF catalysts.

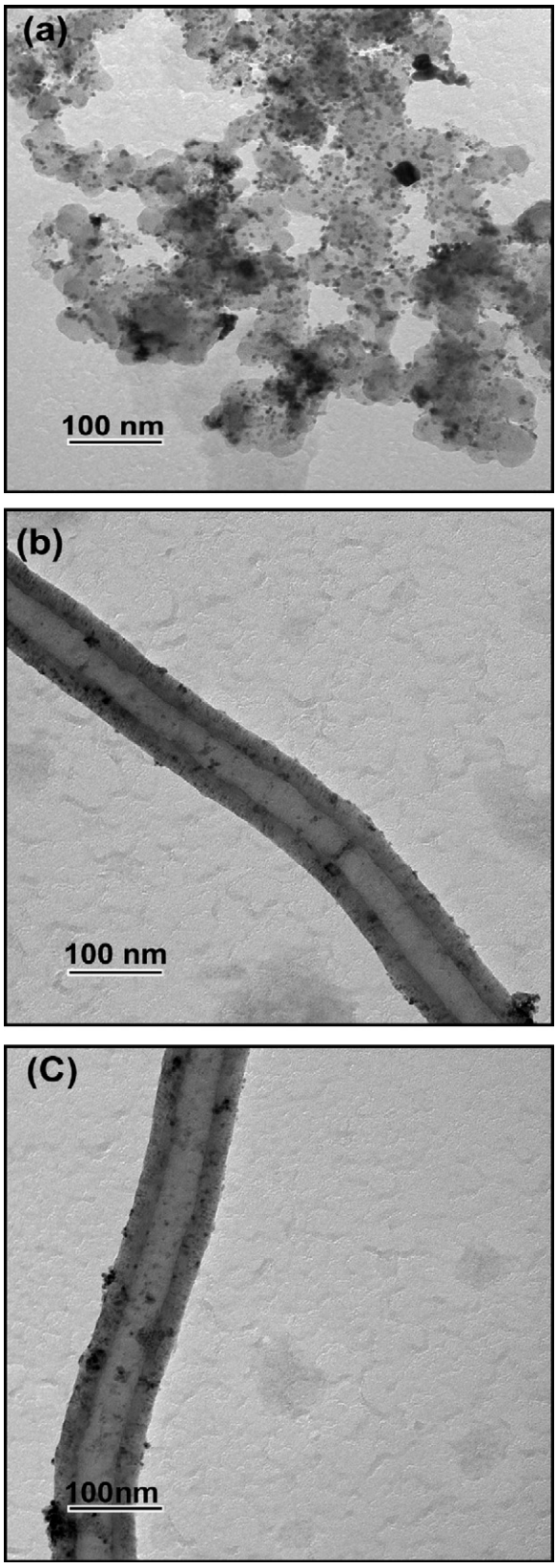

Fig. 3. TEM images of (a) Pd/C and (b and c) Pd–Ni/CNF catalysts.

reasonably uniform on the outer walls of the CNFs. Considering that Pd nanoparticles strongly interact with oxygen atoms, it can be suggested that Pd nucleation centers occur in the proximity of oxygenated defects created during the treatment. Therefore, the improved metal nanoparticle dispersion for the nitric acid-treated

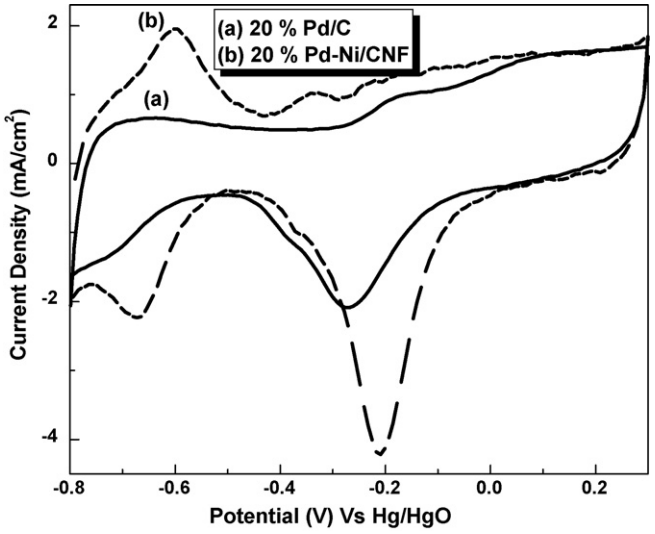

Fig. 4. Cyclic voltammogram of Pd/C and Pd–Ni/CNF electro-catalysts in 1 M KOH with a scan rate of 10 mV s^{-1}, 25 °C.

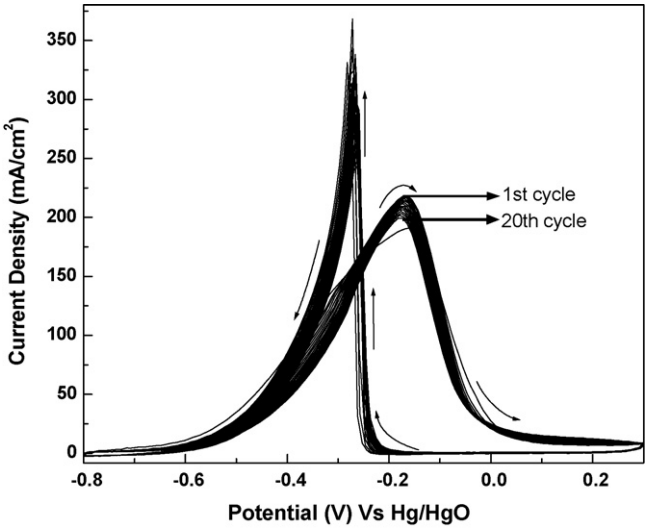

Fig. 5. Cyclic voltammograms of Pd–Ni/CNF electrodes in 1 M KOH/1 M C_2H_5OH solution at a scan rate of 10 mV s^{-1} (20 scans), 25 °C.

CNF can be attributed to the creation of dispersed oxidized vacancies at the CNF-surface by the HNO_3 treatment [31].

The cyclic voltammograms (CV) of Pd–Ni/CNF and Pd/C electrocatalysts in the absence of ethanol are shown in Fig. 4. On the cathodic scan, the palladium oxide layer is reduced, with a reduction peak at −0.270 V. The cyclic voltammetric behavior of the Pd/carbon/GC electrode was a little different from that of palladium electrode reported [32].

The potential region from −800 to −500 mV versus Hg/HgO on the CV curve of the catalyst in background solution is associated with the hydrogen adsorption/desorption [33]. The electrochemical active surface areas (EASAs) of catalysts were measured by integrating the charge on hydrogen adsorption–desorption regions by cyclic voltammetry. These values given in Table 1, can be calculated after the deduction of the double layer region on the CV curves represents the charge passed for the hydrogen desorption, Q_H, and is proportional to the electrochemically active area (EAA) of the electro-catalysts [34]. The value Q_H = 15. 5 mC cm^{-2} for the Pd–Ni/CNF electrode is much higher than 2.7 mC cm^{-2} for the Pd/C electrode.

The cyclic voltammograms of Pd–Ni/CNF catalysts for ethanol oxidation during the first 20 cycles are shown in Fig. 5. The magnitude of reduction in current is lower as the number of cycles increases from 1 to 20. Then the peak current remained almost constant and the current density was hardly changed after 20 cycles. The relatively good stability of the ethanol oxidation current over repetitive potential cycling seems to suggest that surface poisoning by reaction intermediates is insignificant.

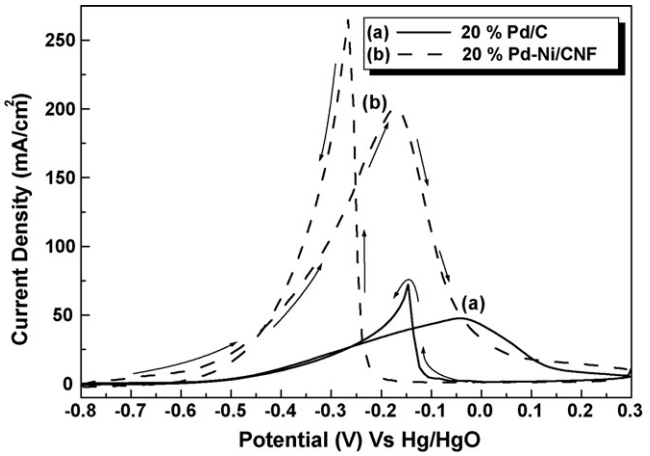

Fig. 6. Cyclic voltammograms of ethanol electro-oxidation on (a) Pd/C and (b) Pd–Ni/CNF electrodes in 1 M KOH/1 M C_2H_5OH solution at a scan rate of 10 mV s^{-1} (recorded after 20 scans), 25 °C.

The typical cyclic voltammograms of Pd/C and Pd–Ni/CNF catalysts for ethanol oxidation in 1.0 M KOH/1.0 M ethanol solution at room temperature are shown in Fig. 6. In the forward scan, the oxidation peak corresponds to the oxidation of freshly chemisorbed species coming from ethanol adsorption. The reverse scan peak is primarily associated with removal of carbonaceous species not completely oxidized in the forward scan than the oxidation of freshly chemisorbed species.

Table 1
Comparison of activity of ethanol oxidation between Pd/C and Pd–Ni/CNF electrodes.

S. no	Electrode	Onset potential (V)	EASA (mC cm^{-2})	Activity[a]			
				Forward sweep		Reverse sweep	
				I (mA cm^{-2})	E (mA cm^{-2})	I (mA cm^{-2})	E (mA cm^{-2})
1	Pd/C	−0.5	2.7	47.8	−0.03	72.5	−0.14
2	Pd/C[b]	−0.524	1.91	28	–	–	–
3	Pd/HCS[b]	–	10.7	90	–	–	–
4	Pd–Ni/CNF	−0.7	15.5	199.8	−0.17	264.5	−0.26
5	Pd–NiO(6:1)/C[c]	−0.62	–	95	−0.08	–	–

[a] Activity evaluated from cyclic voltammogram in 1 M KOH/1 M C_2H_5OH.
[b] From Ref. [32].
[c] From Ref. [33].

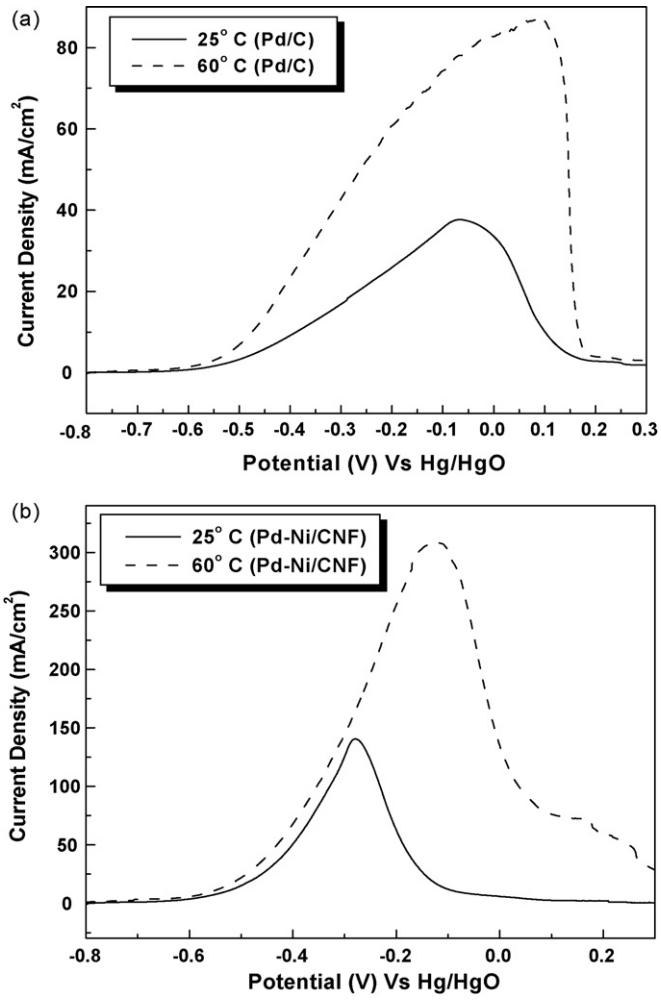

Fig. 7. Linear potential sweep curves: (a) Pd/C catalysts and (b) Pd–Ni/CNF catalysts in 1 M KOH/1 M C_2H_5OH solution with a scan rate of 1 mV s^{-1}, (—) 25 °C and (—-): 60 °C.

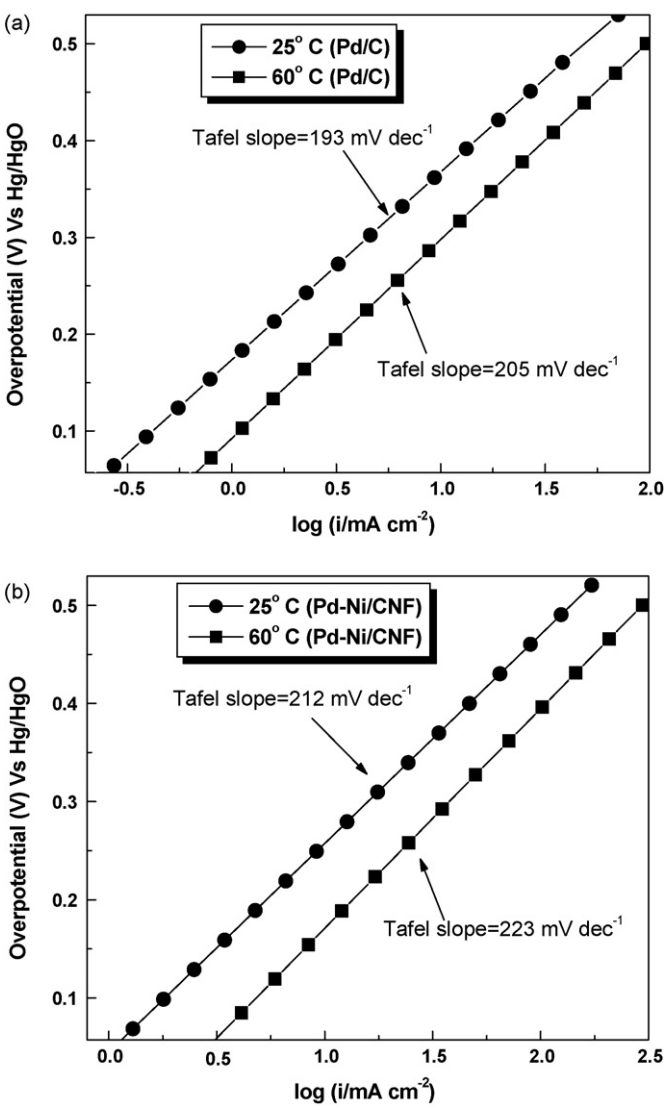

Fig. 8. Tafel plot of (a) Pd/C catalysts and (b) Pd–Ni/CNF catalysts in 1 M KOH/1 M C_2H_5OH solution with a scan rate of 1 mV s^{-1}, 25 and 60 °C.

The Pd–Ni catalyst supported on CNF (Pd–Ni/CNF) catalyst showed a better activity for ethanol oxidation than Pd/C. The onset potential for EOR on Pd–Ni/CNF electro-catalyst was 200 mV more negative in comparison with that of Pd/C electro-catalyst. Similar values for Pd–NiO/C were reported [35]. It is clear that the involvement of Ni significantly increased the catalytic activity at the same Pd loadings. The peak current density for ethanol oxidation is 200 mA cm^{-2} on the Pd–Ni/CNF electrode, was four times higher than on the Pd/C electrode, 47.8 mA cm^{-2}. The forward peak potential for the electro-oxidation of ethanol on the Pd–Ni/CNF electrode was −0.17 V (versus Hg/HgO), lower than −0.03 V (versus Hg/HgO) for Pd/C catalyst. The high peak oxidation current and low anodic peak potential show that Pd–Ni/CNF electro-catalysts were more active than the Pd/C electrode. Moreover, the higher catalytic currents at more negative potentials on Pd–Ni/CNF electro-catalysts could potentially improve the DEFC efficiency. Evaluation of these catalysts in DEFC using anion conducting membranes will be the subject of future research.

The effect of temperature on ethanol oxidation for Pd/C and Pd–Ni/CNF catalysts was investigated by performing linear sweep voltammograms at a scan rate of 1 mV s^{-1} at temperatures 25 and 60 °C (data shown in Fig. 7a and b, respectively). Current density increased significantly with the higher temperature, i.e. peak current density was some three times greater, indicating an increase in reaction kinetics.

The kinetic parameters of ethanol oxidation on Pd/C and Pd–Ni/CNF catalysts were obtained from Tafel plots, shown in Fig. 8. The Tafel slopes for Pd/C catalyst were 193 and 205 mV dec^{-1} at 25 and 60 °C, respectively and for Pd–Ni/CNF catalyst were 196 and 213 mV dec^{-1} at 25 and 60 °C, respectively. The results of Pd/C catalyst are in agreement with the literature [36].

By extrapolating the Tafel line, to the point at where the overpotential equals zero. The exchange current density, i_0, can be obtained. It is evident from the Tafel plot in Fig. 8 that the calculated exchange current density i_0 for the Pd–Ni/CNF catalyst is significantly greater than for the Pd/C catalyst. This data indicates the Pd–Ni/CNF catalyst has a higher activity for ethanol oxidation in alkaline media than the Pd/C catalyst and values are given in Table 2, at the two different temperatures. The exchange current densities for ethanol oxidation on Pd–Ni/CNF electrode were almost two orders higher than that on Pd/C electrodes.

The electrochemical stability of Pd/C and Pd–Ni/CNF electrodes for ethanol electro-oxidation was also investigated by chronoamperometry. Fig. 9 shows the current density–time plots of Pd/C and Pd–Ni/CNF electrodes in 1 M KOH and 1 M ethanol at −0.5 V.

The results indicate that the improvement in the activity of Pd–Ni/CNF electro-catalyst for ethanol oxidation may partly

Table 2
Kinetic parameters of ethanol oxidation on Pd/C and Pd–Ni/CNF electrodes.

S. no	Electrode	Temperature (K)	Tafel slope (mV dec^{-1})	i^o (A cm^{-2})
1	Pd/C	298	193	2.69×10^{-4}
2	Pd/C	333	205	6.8×10^{-4}
3	Pd/C[a]	298	188	2.7×10^{-5}
4	Pd–Ni/CNF	298	212	1.18×10^{-3}
5	Pd–Ni/CNF	333	223	3.0×10^{-3}
6	Pd–NiO/C[a]	298	195	1.8×10^{-4}

[a] From Ref. [11].

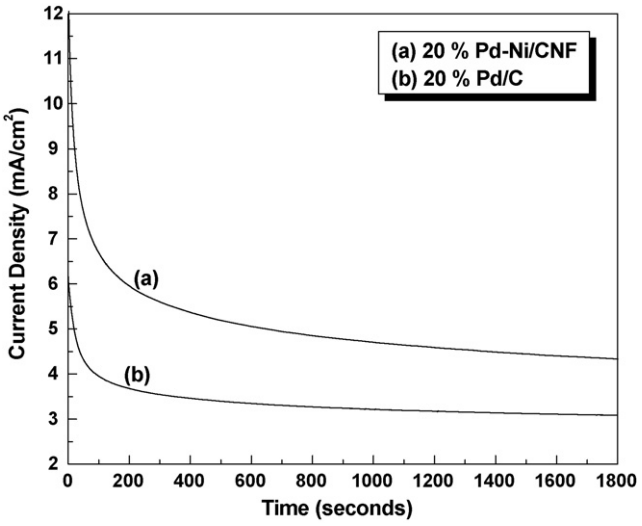

Fig. 9. Current density–time curves at −0.5 V for 1800 s at (a) Pd/C and (b) Pd–Ni/CNF in 1 M KOH/1 M C_2H_5OH solutions, 25 °C.

attributes to the uniform distribution of metal nanoparticles on the CNF support. It is thought that the addition of Ni significantly decreased the overpotential and NiOOH formed on the surface of the catalyst enhances the catalytic activity for ethanol oxidation [37].

4. Conclusions

Well-dispersed Pd–Ni nanoparticle catalysts have been synthesized on carbon nanofibers composite. These catalysts were good materials for ethanol oxidation in alkaline medium and were more active than Pd/C catalysts. The results showed a 200 mV decrease in the onset potential and a threefold enhancement in the peak current density for Pd–Ni/CNF catalyst compared to Pd/C catalyst with the same Pd loading. The enhancements in activity and stability of Pd–Ni/CNF catalyst compared to the Pd/C catalyst can be attributed to the carbon nanofiber support and the addition of Ni to the Pd. The data suggest that Pd–Ni/CNF should be considered a good electro-catalyst material for alkaline direct ethanol fuel cells.

Acknowledgments

EPSRC and DSTL are acknowledged for support of this work.

References

[1] U.B. Demirci, J. Power Sources 169 (2007) 239.
[2] J.S. Spendelow, A. Wieckowski, Phys. Chem. Chem. Phys. 9 (2007) 2654.
[3] A.V. Tripkovic, K.D. Popovic, B.N. Grgur, B. Blizanac, P.N. Ross, N.M. Markovic, Electrochim. Acta 47 (2002) 707.
[4] J.S. Spendelow, G.Q. Lu, P.J.A. Kenis, A. Wieckowski, J. Electroanal. Chem. 568 (2004) 15.
[5] J.L. Cohen, D.J. Volpe, H.D. Abruna, Phys. Chem. Chem. Phys. 9 (2007) 49.
[6] S.L. Chen, M. Schell, Electrochim. Acta 45 (2000) 3069.
[7] A.V. Tripkoic, K.D. Popovic, J.D. Lovic, Electrochim. Acta 46 (2001) 3163.
[8] S.M. Park, N. Chen, N. Doddapaneni, J. Electrochem. Soc. 142 (1995) 40.
[9] F.P. Hu, C.L. Chen, Z.Y. Wang, G.Y. Wei, P.K. Shen, Electrochim. Acta 52 (2006) 1087.
[10] C.W. Xu, P.K. Shen, Y.L. Liu, J. Power Sources 164 (2007) 527.
[11] P.K. Shen, C.W. Xu, Electrochem. Commun. 8 (2006) 184.
[12] N.M. Suleimanov, S.M. Khantimerov, E.F. Kukovitsky, V.L. Matukhin, J. Solid State Electrochem. 12 (2008) 1021.
[13] G.P. Jin, Y.F. Ding, P.P. Zheng, J. Power Sources 166 (2007) 80.
[14] X.-K. Tian, X.-Y. Zhao, L.-D. Zhang, C. Yang, Z.-B. Pi, S.-X. Zhang, Nanotechnology 19 (21) (2008) 215711.
[15] C.W. Xu, Y.H. Hu, J.H. Rong, S.P. Jiang, Y.L. Liu, Electrochem. Commun. 9 (2007) 2009.
[16] C.A. Bessel, K. Laubernds, N.M. Rodriguez, R.T.K. Baker, J. Phys. Chem. B 105 (2001) 1115.
[17] W.Z. Li, C.H. Liang, W.J. Zhou, Q. Xin, J. Phys. Chem. B 107 (2003) 6292.
[18] C. Wang, M. Waje, X. Wang, J.M. Tang, R.C. Haddon, Y.S. Yan, Nano Lett. 4 (2004) 345.
[19] T. Maiyalagan, Appl. Catal. B: Environ. 89 (2008) 286.
[20] T. Maiyalagan, B. Viswanathan, U.V. Varadaraju, Electrochem. Commun. 7 (2005) 905.
[21] T. Yoshitake, Y. Shimakawa, S. Kuroshima, H. Kimura, T. Ichihashi, Y. Kubo, Physica B 323 (2002) 124.
[22] T. Hyeon, S. Han, Y.E. Sung, K.W. Park, Y.W. Kim, Angew. Chem. 42 (2003) 4352.
[23] W.Q. Yang, S.H. Yang, J.S. Guo, G.Q. Sun, Q. Xin, Carbon 45 (2007) 397.
[24] T. Maiyalagan, J. Solid State Electrochem. 13 (2009) 1561.
[25] M.A. Abdel Rahim, R.M. Abdel Hameed, M.W. Khali, J. Power Sources 134 (2004) 160.
[26] J.-P. Tessonnier, D. Rosenthal, T.W. Hansen, C. Hess, M.E. Schuster, R. Blume, F. Girgsdies, N. Pfander, O. Timpe, D.S. Su, R. Schlogl, Carbon 47 (2009) 1779.
[27] T. Maiyalagan, Int. J. Hydrogen Energy 34 (2009) 2874.
[28] P.V. Lakshminarayanan, H. Toghiani, C.U. Pittman, Carbon 42 (2004) 2433.
[29] A. Houdayer, R. Schneider, D. Billaud, J. Ghanbaja, J. Lambert, Synth. Met. 151 (2005) 165.
[30] V. Radmilovic, H.A. Gasteiger, P.N. Ross, J. Catal. 154 (1995) 98.
[31] Y.Q. Cai, A.M. Bradshaw, Q. Guo, D.W. Goodman, Surf. Sci. 399 (1998) L357.
[32] L.D. Burke, J.K. Casey, J. Electrochem. Soc. 140 (1993) 1292.
[33] R. Pattabiraman, Appl. Catal. A 153 (1997) 9.
[34] F.P. Hu, P.K. Shen, J. Power Sources 173 (2007) 877.
[35] C. Liu, Y. Liu, J. Power Sources 164 (2007) 527.
[36] F.P. Hu, G.F. Cui, Z.D. Wei, P.K. Shen, Electrochem. Commun. 10 (2008) 1303.
[37] M. Fleischmann, K. Korinek, D. Pletcher, J. Chem. Soc. Perkin 2 (1972) 1396.